Hindawi
Shock and Vibration
Volume 2024, Article ID 8026402, 16 pages
https://doi.org/10.1155/2024/8026402

Research Article

Accuracy-Improved Fault Diagnosis Method for Rolling Bearing Based on Enhanced ESGMD-CC and BA-ELM Model

Wei Yuan,[1,2] **Fuzheng Liu**,[3] **Hongbin Gu**,[1] **Fei Miao**,[2] **Faye Zhang**,[3] **and Mingshun Jiang**[3]

[1]*College of Civil Aviation, Nanjing University of Aeronautics and Astronautics, Nanjing 211106, China*
[2]*Flying College, Shandong University of Aeronautics, Binzhou 256603, China*
[3]*School of Control Science and Engineering, Shandong University, Jinan 250061, China*

Correspondence should be addressed to Fei Miao; mr_miaofei@bzu.edu.cn

Received 3 April 2023; Revised 6 December 2023; Accepted 24 February 2024; Published 15 March 2024

Academic Editor: Antonio Batista

The current methods for early fault diagnosis of rolling bearing have some flaws, such as poor fault feature information and insufficient fault feature extraction capability, which makes it challenging to guarantee fault diagnosis accuracy. In order to increase the accuracy of fault diagnosis, it proposes a new fault diagnosis method based on enhanced Symplectic geometry mode decomposition with cosine difference factor and calculus operator (ESGMD-CC) and bat algorithm (BA) optimized extreme learning machine (ELM). The vibration signal is first decomposed into a number of Symplectic geometry components (SGCs) by SGMD. The number of iterations is reduced by the cosine difference factor, which also successfully separates the noise components from the effective components. The calculus operator is adopted to strengthen the weak fault features, making it simple to extract. The fault feature vectors are calculated by the power spectrum entropy-weighted singular values. Finally, the ELM model optimized by BA iteratively is performed as the final classifier for fault classification. The simulation and experiments demonstrate that the proposed method has a better degree of fault diagnostic accuracy and is effective at extracting the rich fault information from vibration signals.

1. Introduction

Bearings are commonly used as critical components of mechanical machinery. Failure of a component may cause financial loss or endanger human life. As a result, a more comprehensive examination of rolling bearing defect diagnostic technology is critical for ensuring the dependable operation of mechanical equipment and minimizing accidents [1–3]. In normal operation, the signal generated by a rolling bearing is steady; however, the signal produced following a failure is nonstationary. When a failure occurs, the bearing will vibrate and impact severely, which will cause pulse and random signals to be produced. The extraction and identification of fault signals will be significantly hampered by the creation of pulse signals, which will interact with and bury the fault characteristic signal [4, 5].

Numerous signal decomposition techniques have been presented in order to enhance the capability of feature extraction from vibration signals. Empirical mode decomposition (EMD) [6] is a popular adaptive signal processing technique that extracts more information from a signal by subdividing it into various IMFs. It is utilized in a variety of industries [7–9]. Although EMD can efficiently process nonlinear signals, it suffers from substantial mode aliasing and end effect issues because it relies too heavily on the interpolation process of the carrier envelope. The authors of [10] generate the final decomposition component, known as ensemble EMD (EEMD), by recycling EMD and adding Gaussian white noise to address the aforementioned issue. However, the noise robustness still has two nonadaptive parameters, which makes it less than ideal. Local mean decomposition (LMD) [11] is enhanced by EMD as a foundation which is frequently employed in the identification of bearing faults [12, 13]. In recent years, variable mode decomposition (VMD), a technique that can successfully identify fault features from vibration data, has

received a lot of attention [14]. Two crucial elements that affect the results of VMD decomposition are the number of modal decompositions and the penalty factor. The authors of [15, 16] and others have optimized the selection of parameters and achieved certain application effects. SGMD proposed by PAN [17] can adaptively partition time series into SGCs of various independent modes based on Symplectic geometry theory, improving the feature extraction capability of fault information. SGMD is effective at processing mechanical fault vibration signals because it prevents modal aliasing and preserves the intrinsic properties of time series. However, there are still several theoretical and practical issues with SGMD that need to be fixed, such as the flaws of reconstruction constraints and decomposition errors. The enhanced ESGMD-CC is proposed in this paper as a solution to these issues. To accurately distinguish between the noisy components and the effective components, the cosine value is used to calculate how similar the two stacked components are, and the difference factor is adopted to set a limit on the number of repeats. Decomposition components are processed by a calculus operator, which is convenient for enhancing weak fault characteristics and making them simple to extract, successfully resolving the issue of the SGMD algorithm's poor ability to recognize fault features.

The enhanced ESGMD-CC decomposition leaves a significant amount of fault-related data in the enhanced Symplectic limiting components (ESLCs). However, a suitable technique is still needed to extract defect features from these decomposed components. Different approaches have been explored to address this issue. Ren et al. [18], for instance, compute multiscale permutation entropy to produce eigenvectors. Zhang et al. [19] also derive the feature vector from the permutation entropy. Liu et al. [20] create the eigenvectors by the fault energy moment values. These techniques are effective in extracting fault features that precisely show signal properties. These methods do not account for the fact that some of the decomposed components are noisy and require additional processing because of their computational complexity. Considering these problems, this paper adopts the PSE-weighted singular values as the fault feature vectors to effectively overcome the above problems and accurately extract the fault feature vectors for later fault classification.

After feature extraction, it is essential to adopt the proper classification methods to quickly identify probable rolling bearing defects. Machine learning has been the subject of extensive research by academics both domestically and overseas [21]. Based on the machine learning diagnosis approaches, it first extracts distinctive sample features by signal analysis and other technologies, and then classifiers such as backpropagation (BP), random forest (RF), support vector machine (SVM), and extreme learning machine (ELM) [22–24] should be performed to identify the mapping relationship between fault feature components and labels. In [25], the ideal weight and threshold of the BP are optimized using the genetic algorithm's global search advantage. The authors of [26] proposed a signal processing strategy that combines RCHFE and RF for planetary gearbox failure diagnosis, and by combining simulation and experimental signals, it demonstrated the superiority of the proposed RCHFE-RF method. Liu et al. [27] applied an improved EMD method in bearing fault diagnosis. According to the aforementioned research, these classification algorithms have a large number of parameter settings, extreme values, a sluggish training speed, and other issues that restrict their application in defect diagnosis. ELM is a learning technique for feedforward neural networks with a single hidden layer [28]. It is suitable for application in fault diagnosis since it has great generalization capabilities and a quick learning rate. In [29], a new deep kernel limit learning machine (DK-ELM) was proposed. For fault classification, the kernel is utilized in place of the conventional ELM, and better diagnostic performance is obtained in terms of diagnostic accuracy and flexibility in working situations. Input weights and bias are selected at random during the ELM computation, which will have an impact on the stability and precision of fault diagnosis. To prevent the impact of random selection on the outcomes of the diagnostic, appropriate optimization techniques must be added, such as particle swarm optimization [30], ant colony optimization [31], and artificial fish swarm algorithm [32].

BA [33] is a brand-new method using frequency tuning mode. It is a suitable optimization technique created by modeling bat features. It is easy to construct, quickly converge, and benefit from distributed and parallel computation. From the aspect of fault diagnosis, in order to find the optimal connection weights and neuron bias in the ELM model better and faster, this paper intends to use BA to optimize the weights and bias in the ELM model to achieve a better calculation effect.

To overcome these concerns, this work provides an enhanced ESGMD-CC theory and BA-ELM model. To properly separate the noisy and effective components, the cosine difference factor is employed to minimize the number of iterations for the SGCs produced by the SGMD. The calculus operator is used to improve and simplify the extraction of the weak defect feature. Furthermore, the fault feature vectors are built using power spectrum entropy-weighted singular values, which effectively tackles the issue of poor feature identification. The BA then repeatedly optimizes the ELM model to discover the appropriate input weights and neuron bias faster and more efficiently, resulting in enhanced fault classification performance.

In summary, the main contributions of this paper can be summarized as follows:

(1) An improved ESGMD-CC technique is given based on Symplectic geometry similarity transformation. This approach effectively extracts rich fault features from signals and has better vibration signal decomposition performance.

(2) The cosine difference factor is performed to limit the number of iterations of SGMD, distinguish the noise components, and reduce the feature dimension. The weak fault features are enhanced by the calculus operator to make it easy to extract. The feature mapping method by power spectrum entropy-weighted singular values is adopted, and the

enhanced ESGMD-CC algorithm is fully combined to effectively extract the fault features of the signal.

(3) BA is performed to iteratively optimize the input weights and bias in the ELM model, and its diagnosis effect is better than that of traditional BP, SVM, and ELM models.

The rest of this paper is organized as follows. Section 2 introduces the signal decomposition method of enhanced ESGMD-CC and the feature extraction method. Section 3 introduces BA-ELM theory. Section 4 introduces the overall process of the fault diagnosis algorithm. In Section 5, the simulated signal is used to verify the effectiveness of the proposed signal decomposition method. Section 6 presents the experimental results and corresponding analysis of rolling bearing fault diagnosis based on enhanced ESGMD-CC and BA-ELM. Finally, according to the work done in this paper, it is summarized in Section 7.

2. Signal Decomposition and Feature Extraction

2.1. SGMD Theory. The algorithm of the traditional SGMD is described as follows:

(1) Phase space reconstruction

Suppose an original time series signal $(x = x_1, x_2, \cdots, x_n)$, which n represents the length of the signal. According to the Takens embedding theory, the trajectory matrix X can be constructed as shown in the following equation:

$$X = \begin{bmatrix} x_1 & x_{1+\tau} & \cdots & x_{1+(d-1)\tau} \\ \vdots & \vdots & & \vdots \\ x_m & x_{m+\tau} & \cdots & x_{m+(d-1)\tau} \end{bmatrix}, \tag{1}$$

where d is the embedded dimension, τ is the delay time, and $m = n - (d-1)\tau$. The method in [17] is used to adaptively determine the value d by calculating the power spectral density of the original time series.

(2) QR decomposition of the Symplectic orthogonal matrix

In order to obtain the Hamiltonian matrix, the covariance matrix A is obtained through the autocorrelation analysis of the trajectory matrix X:

$$A = X^T X. \tag{2}$$

Then, the Hamiltonian matrix M is obtained through matrix A:

$$M = \begin{pmatrix} A & 0 \\ 0 & -A^T \end{pmatrix}. \tag{3}$$

It is proved that there is a Householder matrix $H = \mathrm{diag}(Q, Q)$, in which the matrix Q can be composed of real symmetric matrix A, and the matrix H is also a Symplectic geometry orthogonal matrix:

$$\begin{aligned} HMH^T &= \begin{pmatrix} Q & 0 \\ 0 & Q \end{pmatrix} \begin{pmatrix} A & 0 \\ 0 & -A^T \end{pmatrix} \begin{pmatrix} Q & 0 \\ 0 & Q \end{pmatrix}^T \\ &= \begin{pmatrix} QAQ^T & 0 \\ 0 & -QA^TQ^T \end{pmatrix} \\ &= \begin{pmatrix} B & 0 \\ 0 & -B^T \end{pmatrix}, \end{aligned} \tag{4}$$

where the matrix B is an upper triangular Hessenberg matrix, which is easy to obtain $\lambda(A) = \lambda(B) = \lambda^2(X)$. The eigenvalues of the matrix B are $\lambda_1, \lambda_2, \cdots, \lambda_d$. According to the properties of the Hamiltonian matrix, the eigenvalues of the matrix X are as follows:

$$\sigma_i = \sqrt{\lambda_i}\,(i = 1, 2, \cdots d), \tag{5}$$

where $\lambda_1 > \lambda_2 > \cdots > \lambda_d$, λ_i is arranged from high to low. The distribution of λ_i represents the spectral distribution of matrix A. The smaller values are usually considered as the noise components. $Q_i\,(i = 1, 2, \cdots, d)$ are the eigenvectors corresponding to the eigenvalues of matrix A. The transformation coefficient matrix S is calculated by equation (6) through the eigenvector Q and the trajectory matrix X:

$$S_i = Q_i^T X^T\,(i = 1, 2, \cdots, d). \tag{6}$$

Furthermore, the reconstruction matrix Z is calculated by equation (7) through the eigenvector Q and transformation coefficient matrix S:

$$Z_i = Q_i S_i\,(i = 1, 2, \cdots, d). \tag{7}$$

The reconstruction matrix Z is composed of d groups initial single components reconstruction matrix Z_i:

$$Z = Z_1 + Z_2 + \cdots + Z_d. \tag{8}$$

(3) Diagonal averaging transformation

The dimension of the reconstructed matrix Z_i obtained is $m \times d$. By diagonal averaging, the reconstructed matrix Z_i can be transformed into a one-dimensional time series $Y_i(y_1, y_2 \cdots, y_n)$ with a length of n. Such time series can obtain d groups in total, and the sum of these d groups of time series is equal to the original time series x.

The specific transformation process of the diagonal average is as follows:

For the element $z_{ij}\,(1 \le i \le m, 1 \le j \le d)$ in matrix Z_i, let $d^* = \min(m, d)$, $m^* = \max(m, d)$, $m = n - (d-1)\tau$. If $m < d$, let $z_{ij}^* = z_{ij}$, otherwise, $z_{ij}^* = z_{ji}$.

Then, the element $y_k\,(k = 1, 2, \cdots, n)$ in the corresponding time series Y_i is calculated as shown in the following equation:

$$y_k = \begin{cases} \dfrac{1}{k}\displaystyle\sum_{p=1}^{k} z^*_{p,k-p+1}, & 1 \le k < d^*, \\ \dfrac{1}{d^* \sum_{p=1}^{d^*} z^*_{p,k-p+1}}, & d^* \le k \le m^*, \\ \dfrac{1}{n-k+1}\displaystyle\sum_{p=k-m^*+1}^{n-m^*+1} z^*_{p,k-p+1}, & m^* < k \le n. \end{cases} \tag{9}$$

By equation (9), the initial single components reconstruction matrix Z_i is converted into a one-dimensional time series $Y_i(y_1, y_2 \cdots, y_n)$. Therefore, by diagonal averaging, the trajectory matrix X can be converted into a series of d groups with a length of n:

$$Y = Y_1 + Y_2 + \cdots + Y_d. \tag{10}$$

It is easy to know that the sum of these series is the original time series x.

2.2. ESGMD-CC. Several initial single components $(Y = Y_1 + Y_2 + \cdots + Y_d)$, which typically contain a lot of noise components, are obtained by the SGMD technique. Importantly, it is first to separate the noise components from the effective components. To reduce the number of iterations and effectively separate the noise components from the effective components, the cosine difference factor is applied in this case. Further processing is necessary because the eigenvectors that correspond to significant eigenvalues in the noise signal also contain noise components. A calculus operator is adopted to enhance weak fault characteristics so that they may be easily extracted, preventing weak fault features from being masked by background noise.

(1) Separation of noise components

First, we sum the decomposed components. For the obtained d groups initial single components $(Y_1, Y_2, \cdots, Y_d)$, the sum components S_k are obtained by calculating the sum of the previous k group components:

$$S_k = \sum_{i=1}^{k} Y_i \ (k = 1, 2, \cdots, d). \tag{11}$$

Second, we calculate the cosine values between adjacent components. For the obtained k groups sum components S_k, calculate their cosine values C_i according to the following equation:

$$C_i = \cos\theta_{k,k+1} = \frac{S_k \cdot S_{k+1}}{\|S_k\| \cdot \|S_{k+1}\|} \ (i, k = 1, 2, \cdots, d-1). \tag{12}$$

Finally, we calculate the difference factor. Combined with the characteristics of cosine values, the difference operation can highlight the turning point where the stack components tend to be stable. The cosine difference factor CS_i is constructed by the following equation:

$$\mathrm{CS}_i = \left|\left(C_{i+1} - C_i\right)\right| < \varepsilon_e. \tag{13}$$

When the values of CS_i change steadily and reach the preset threshold value ε_e which tends to zero, the former z groups components can be selected as the effective components. Before the z point, it contains a lot of useful information about the original signal. After the z point, it can be regarded as noise components.

The original signal x is decomposed into:

$$\begin{aligned} x &= \sum_{i=1}^{z} Y_i + g_z, \\ g_z &= \sum_{i=z+1}^{d} Y_i, \end{aligned} \tag{14}$$

where g_z is the sum of the noise components after the turning point z.

(2) Enhancement of limiting components

Differential and integral signals can enhance fault characteristics through research. The calculus operator is applied to the processing of signal components in order to fully exploit the benefits of differentiation and integration. The significance is that the effect features can be made more visible by the calculus operator to diminish low-frequency noise components, strengthen high-frequency beneficial components, and emphasize the transient components. So weak fault features are strengthened and made easier to extract.

It gives the differential result of the discrete signal $Y(n)$ in the following equation:

$$D(Y(n)) = \frac{(Y(n) - Y(n-1))}{\Delta t}, \tag{15}$$

where $\Delta t = 1/f_s$ and f_s is the sampling frequency。

It gives the integral result of the discrete signal $Y(n)$ in equation (15):

$$I(Y(n)) = \frac{\Delta T(Y(n) + Y(n - \Delta T))}{2}, \tag{16}$$

where ΔT is the step factor. If it is set to 1, equation (16) can be simplified as follows:

$$I(Y(n)) = \frac{(Y(n) + Y(n-1))}{2}. \tag{17}$$

By combining the differential and integral equations, the calculus operator of discrete signal $Y(n)$ can be obtained as follows:

$$\begin{aligned} ca(Y(n)) &= I(D(Y(n))) \\ &= I(Y(n) - Y(n-1)) \\ &= \frac{(Y(n) - Y(n-2))}{2}. \end{aligned} \tag{18}$$

For the reserved first z groups effective components, the calculus operator is performed for signal enhancement, which can give full play to the advantages of differential and integral. To simplify the calculation, Δt and ΔT in equations (15) and (16) are both set to 1, so the ESLCs are as follows:

$$\begin{aligned}\mathrm{ESLC}_i &= ca\left(Y_i(n)\right)\\ &= \frac{\left(Y_i(n) - Y_i(n-2)\right)}{2}.\end{aligned} \tag{19}$$

As an adaptive signal decomposition method, ESGMD-CC has strong robustness and is suitable for processing fault signals with background noise and weak fault characteristics.

2.3. Feature Extraction: Power Spectrum Entropy-Weighted Singular Values. Following the decomposition and reconstruction of rolling bearing vibration signals by the aforementioned ESGMD-CC algorithm, a number of ESLCs that are rich in fault-related data can be retrieved. To extract defect features from these decomposed components, a suitable technique is still required. Singular value decomposition (SVD) has a low computing complexity, is effective at extracting these fault features, and accurately reveals the signal's feature information. It is appropriate for feature extraction of the ESLCs-based matrix. The singular value feature vectors are weighted at the same time by the power spectrum entropy which can reflect the complexity of the signal. The following are the steps:

(1) ESGMD-CC is first adopted to decompose the vibration signals, which can be decomposed into multiple ESLCs, recorded as $e_i(t), i = 1, 2, \ldots, h$

(2) SVD is performed on the row vector matrix composed of ESLCs to obtain the singular value matrix E_i:

$$E_i = \mathrm{SVD}\left(\left[e_1(t), e_2(t), \ldots, e_h(t)\right]^T\right). \tag{20}$$

(3) Fourier transforms the component $e_i(t) = (e_{i1}, e_{i2}, \ldots, e_{in})$ of each ESLC to obtain the frequency domain signal $X_i(\omega_r)$, where ω_r is a spectrum, then the power spectrum $P_i(\omega_r)$ is as follows:

$$P_i(\omega_r) = \frac{1}{2\pi n}\left|X_i(\omega_r)\right|^2. \tag{21}$$

According to Parseval's theorem, energy is conserved in the transformation from the time domain to the frequency domain, so it can be written as follows:

$$\left|\sum_{j=1}^{n} e_{ij}\right|^2 = \left|\sum_{r=1}^{n} P_i(r)\right|^2. \tag{22}$$

$P_i(r)$ can be regarded as the energy distribution of $e_i(t)$ in the frequency domain, so the power spectrum entropy PS_i can be defined as follows:

$$\mathrm{PS}_i = -\sum_{r=1}^{n} H_{ir} \ln H_{ir}, \tag{23}$$

where H_{ir} is the proportion of the r-th power spectrum component in $e_i(t)$, and its calculation is as follows:

$$H_{ir} = \frac{P_i(r)}{\sum_{r=1}^{n} P_i(r)}. \tag{24}$$

(4) According to the values of power spectrum entropy, the weighted matrix W_i is constructed by

$$\begin{cases} g = \mathrm{PS}_{\max} - \mathrm{PS}_{\min}, \\ W_i = \dfrac{\mathrm{PS}_i - \mathrm{PS}_{\min}}{g}, \end{cases} \tag{25}$$

where $\mathrm{PS}_{\max}$ is the maximum value in the power spectrum entropy and PS_i and $\mathrm{PS}_{\min}$ are the minimum value in the power spectrum entropy PS_i.

Using the weighted matrix and according to equation (26), the singular value feature vectors E_i are weighted, and finally, the power spectrum entropy-weighted singular values ET_i are obtained as follows:

$$\mathrm{ET}_i = W_i \times E_i \, (i = 1, 2, \ldots, h). \tag{26}$$

The complete process of the signal decomposition and the feature extraction is shown in Figure 1.

3. The Establishment of the BA-ELM Classifier

ELM theory and BA theory are introduced initially in this section. The classical ELM acquires input weight and bias at random, and the model's prediction accuracy needs to be increased. However, based on the robust global search capability of the BA, the input weight and bias of ELM are regarded as each bat of BA to plan the optimal path and obtain the global optimal solution to optimize the input weight and bias in ELM, thereby improving the precision and generalization capability of the classification model.

3.1. ELM Theory. In its most basic form, ELM is a single-layer neural network. Comparatively, its structure is simpler, and it operates more quickly. The most remarkable aspect of the ELM theroy is that weights and biases between layers do not require predefined settings. Figure 2 depicts the ELM network structure.

The ELM algorithm uses functions to produce the hidden layer neuron bias and the connection weights between the input layer and the hidden layer. To get the best result during training, only the hidden layer's number of neurons needs to be set. The connection weight between the input layer and the hidden layer in the model is ω, the connection weight between the hidden layer and the output layer is β, the total number of training samples is Q, the output of the ELM model is T, and the activation function is g. The hidden layer output matrix H can be solved by the following equation:

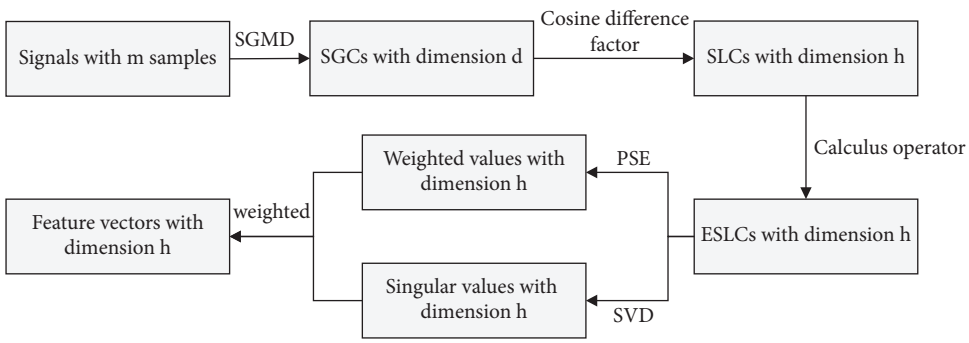

Figure 1: The complete process of the signal decomposition and the feature extraction.

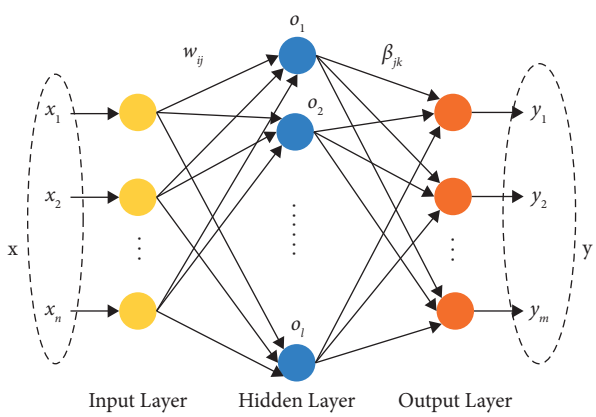

Figure 2: The network structure of the ELM model.

$$H\beta = T'. \tag{27}$$

The connection weights β between the hidden layer and the output layer can be found by resolving the $\min_{\beta}\|H\beta - T'\|$ the equation's least squares solution where $g(x)$ is an infinitely differentiable function. At this point, it changes to the following procedure for solving the weight matrix $\widehat{\beta}$ of the output layer:

$$\widehat{\beta} = H^{+}T, \tag{28}$$

where H^{+} is the generalized inverse of the output matrix H. At present, the singular value decomposition method is commonly used to solve the generalized inverse matrix H^{+}. The singular value decomposition method can effectively ensure that whether $H^{T}T$ is a singular matrix that not can be run, and the running speed is faster than the forward overlapping method. The specific solution is shown in the following equation:

$$\widehat{\beta} = \left(H^{T}T\right)^{-1}H^{T}T. \tag{29}$$

It can be seen that the ELM algorithm is simple to solve and easy to implement. Compared with the traditional gradient descent algorithm, the ELM model has the following advantages: (1) the activation function of the model can use a discontinuous function; (2) the model has good generalization ability; (3) the model can effectively avoid the local minimum problem of traditional gradient descent algorithm; (4) the model only needs to manually set the number of hidden layer neurons, which can effectively improve the experimental efficiency.

In theory, ELM can achieve the lowest training error. Only the number of neurons must be taken into account when utilizing ELM for pattern recognition. The stability and accuracy of fault detection will be impacted since the input weight and bias of the ELM are generated by functions, which have some randomness. In order to optimize it, a suitable algorithm must be included.

3.2. BA-ELM Model. BA is a new intelligent algorithm. It uses the method of frequency tuning and was first proposed by Yang. It is also an intelligent optimization method designed by simulating the characteristics of bats. It has the advantages of simple model construction, fast convergence, and distributed and parallel computations. Because the initial position, pulse frequency, loudness, flight speed, and other factors of bat individuals are different, the final optimized position is also different. All optimization results are actually the optimal individual and its location.

Due to the poor stability of a single ELM model, the parameters that may be selected during ELM model training cannot meet the needs of model stability diagnosis. An important reason for the instability of ELM model prediction results is that the input weight and hidden layer bias of ELM are artificially set, which are generally assigned by random calculation functions, and the input weight and hidden layer bias thus obtained may not meet the requirements of fault classification.

In order to better search for the optimal input weight and bias in the ELM model to achieve better classification accuracy and generalization capability, the BA is introduced to modify the input weights and hidden layer bias of ELM, so as to build the BA-ELM model. Compared with simple ELM, the complexity of the BA-ELM model is slightly increased, but the stability of ELM is greatly improved to achieve a better classification effect. The building steps of the BA-ELM model are as follows, and the flowchart is shown in Figure 3.

(1) The ELM single hidden layer neural network structure is constructed, and the input weight and hidden layer bias are initialized.

(2) The input weight and hidden layer bias are transferred to the bat individual position in BA, the relationship between the two is established, and the sample data are input into the BA-ELM model.

(3) We update the two important parameters of BA, namely, frequency and speed, to get the next position of the corresponding bat individual.

(4) We evaluate the next position of the bat. The evaluation standard is the classification experiment error of ELM. We transfer the value of this position to the ELM part. Based on the sample data, we use the generalized inverse matrix to calculate the classification results and error indicators on the sample data. This error indicator is the evaluation standard of bat position. The error index value is transferred to the BA, and the error value is lower than the error value corresponding to the current position of the bat, which means that the next position of the bat is better, and the bat individual flies to the next position. On the contrary, the individual bat remains in its current position.

(5) When the termination conditions of the BA are met, the optimal bat individual position in the current BA dataset is transferred to ELM, that is, the optimal input weight and hidden layer bias that can be obtained by the current ELM, and then, the output weight is obtained through the generalized inverse matrix, so as to complete the construction of the BA-ELM classification model, and the validity of the model is verified through further prediction experiments.

4. Overall Process of the Proposed Fault Diagnosis Method

The comprehensive method that combines the ESGMD-CC algorithm and the BA-ELM model discussed above has not yet been thoroughly explained in the context of diagnosing rolling bearing faults. Data acquisition, vibration signal decomposition and feature extraction, model construction, and fault diagnosis make up its four primary stages. In this study, the original signals are divided into numerous ESLCs by the ESGMD-CC method. The power spectrum entropy-weighted singular values are extracted as the fault feature vectors for the acquired ESLCs. The BA technique is then performed to iteratively optimize the ELM model's parameters to get the ideal input weights and bias. Finally, the training and diagnostic assignments are carried out by the BA-ELM model. The technical route of this paper is shown in Figure 4.

5. Simulated Vibration Signal Analysis

In order to verify the effectiveness of the proposed method in fault diagnosis, and combined with the actual working environment, the rolling bearing vibration signal submerged in the noise background is simulated. The simulated signal of the rolling bearing fault is established as shown in the following equation:

$$x(t) = x_0 e^{-\varepsilon\omega_n t} \sin \omega_n \sqrt{1-\varepsilon^2}\, t, \tag{30}$$

where the displacement constant $x_0 = 5$, damping coefficient $\varepsilon = 0.15$, system natural frequency fn = 2500 Hz, and fault period $t_0 = 0.01$, so the fault characteristic frequency of the rolling bearing is fg = 100 Hz. Generally, rolling bearings work under strong background noise. Therefore, strong background Gaussian white noise with SNR = −10 dB is added to $x(t)$. The time-domain waveform of the simulated signal is shown in Figure 5, and the envelope spectrum of the simulated signal is shown in Figure 6.

Direct observation of the modulation information of a bearing fault from Figure 5 is not possible. The envelope spectrum analysis in Figure 6 cannot reveal the appropriate fault characteristic frequency of the bearing fault due to the significant background noise addition. The fault characteristic frequency is surrounded by interference peaks of intense background noise, and the characteristic fault is masked by the strong noise components, which reduces the precision of fault identification. To decrease noise and decompose the rolling bearing simulated signal, it is, therefore, required to use the proper signal analysis technique. This will enable the presentation and extraction of fault information. The decomposition methods of VMD and conventional SGMD are used to decompose the original signals. They are shown in Figures 7 and 8, respectively. In this paper, the previously proposed ESGMD-CC approach is performed to decompose and analyze the simulated signal, and the decomposed components are shown in Figure 9.

It is impossible to immediately observe the rolling bearing's modulation information decomposition components. As a result, the envelope spectrum analysis method is utilized to extract the fault characteristic frequency from the envelope spectrum of the effective components acquired. Figures 8 and 9 illustrate how the first component contains the majority of the main features for the SGMD and ESGMD-CC deconstructed components. They are chosen for envelope spectrum analysis as useful components as a result. The envelope spectrum analysis diagrams by the above methods are shown in Figures 10–12. The fault frequency and its frequency multiplication have clear peaks in Figure 12, and there are just a few interference components in the surrounding frequency, which can indicate that there is a bearing fault in the simulated signal.

6. Experimental Verification

6.1. Experimental Equipment and Data Preparation. In this section, the CWRU rolling bearing vibration dataset and the HFZZ-II rotating machinery fault diagnosis simulation platform vibration dataset are selected for analysis and verification.

The CWRU rolling bearing vibration platform is shown in Figure 13. It includes a 2 hp motor, torque encoder, dynamometer, and electronic control equipment which is not shown. The EDM technology is utilized to simulate the motor bearing inner race fault, outer race fault, and ball fault. One of the bearing positions is located at the motor

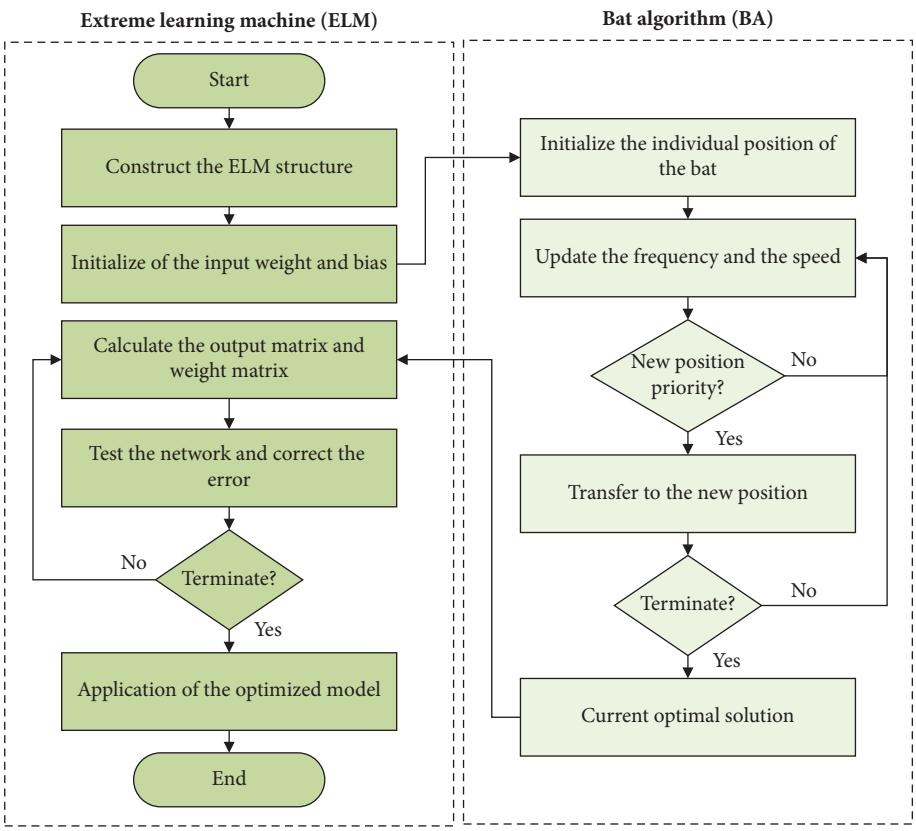

Figure 3: The flowchart of the BA-ELM.

drive end, and the other is located at the fan end. The sampling frequency is 12 KHz. This section sets 11 fault types including normal state (NM), inner race fault (IF), outer race fault (OF), and ball fault (BF), and it consists of 1 normal state and 5 drive end (DE) faults (IFDE, BFDE, OFDE@3, OFDE@6, and OFDE@12), 5 fan end (FE) faults (IFFE, BFFE, OFFE@3, OFFE@6, and OFFE@12), with labels of 0–10, respectively. Each fault includes 1024 sampling points, and 80 groups of data are selected and distributed to the training set and test set with a ratio of 1 : 1.

The HFZZ-II experimental device of the rotating machinery fault diagnosis platform is shown in Figure 14. It is composed of a three-phase AC asynchronous motor, motor control system, bearing pedestal, accelerometer, and data acquisition instrument. The bearing is N205. Among them, two IEPE piezoelectric accelerometers with the model of 1A111E and the acquisition frequency of 12.8 kHz are installed on the tested bearing pedestal. Four types of data, including normal state, inner race fault, ball fault, and outer race fault, are selected for verification, with labels of 0–3, respectively. 80 groups of data are also set for each fault type and allocated to the training set and test set. The physical diagram and time-domain waveform of each fault are shown in Figures 15 and 16.

6.2. Experimental Setup. After data preparation, evident features cannot be separated by the rolling bearing's time-domain waveform, necessitating the use of the proposed method for fault detection. This paper conducts corresponding comparative tests from the following aspects in order to thoroughly assess the performance of the proposed method:

(1) In order to evaluate the advantages of the overall feature extraction method, the enhanced ESGMD-CC is combined with the power spectrum entropy-weighted singular values feature extraction and compared with the traditional mechanical vibration signal decomposition methods EEMD, LMD, and VMD. At the same time, in order to evaluate the necessity of the proposed constraint conditions based on the cosine difference factor and calculus operator, the traditional SGMD method is also compared.

(2) In order to verify the advantages of BA optimized ELM classification model, it is compared with the traditional ELM model, and several common classification models such as BP and SVM are also compared.

(3) In order to evaluate the performance of the proposed method in terms of time consumption, the calculation time of the proposed method is compared with that of other methods in different stages of the diagnosis process.

(4) In order to evaluate the performance of the whole fault diagnosis process, the proposed fault diagnosis method is compared with some work published in the literature.

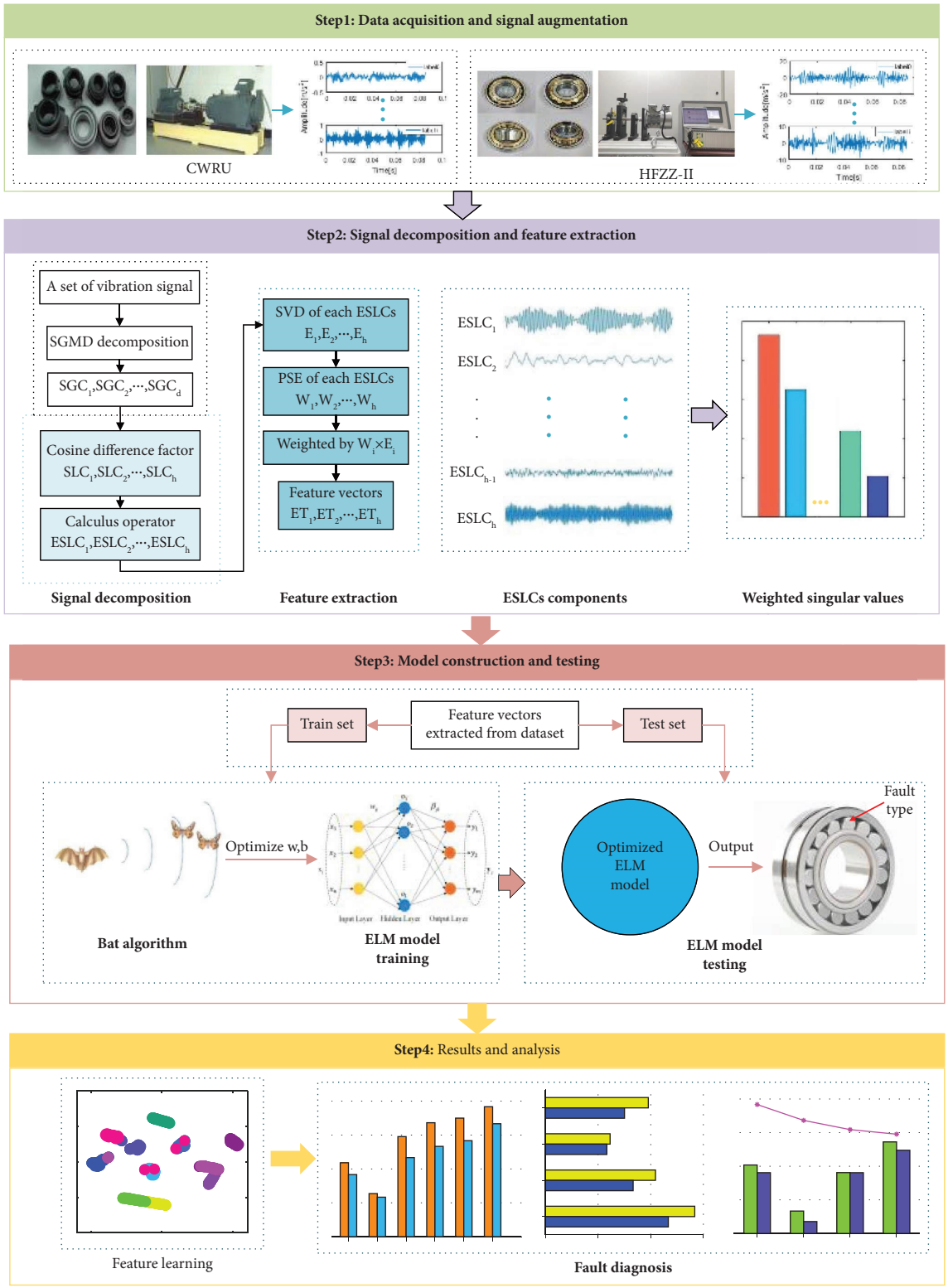

Figure 4: The technical route of this paper.

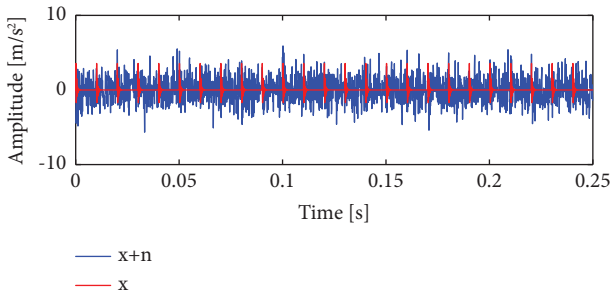

Figure 5: The time-domain waveform of the simulated vibration signal.

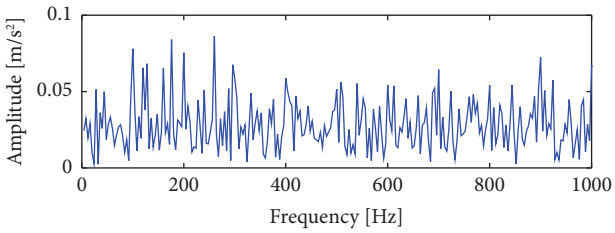

Figure 6: The envelope spectrum of the simulated vibration signal.

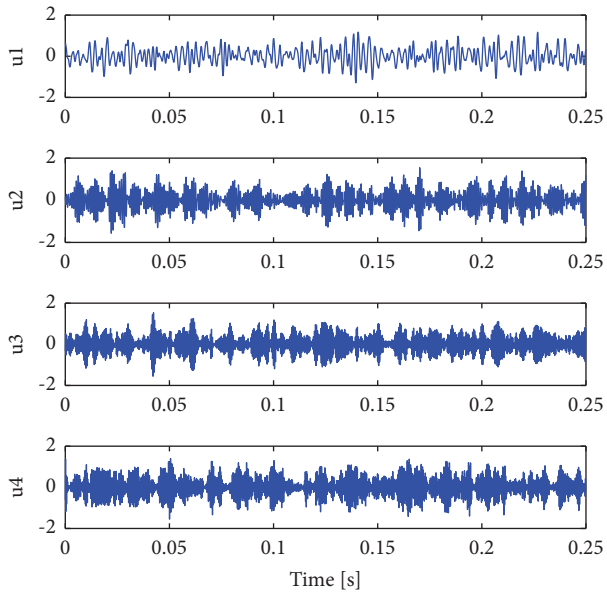

Figure 7: The decomposition components of the VMD.

Four groups of related comparative experiments were carried out in accordance with the aforementioned four levels. In the aforementioned four groups of studies, each group carried out ten separate experiments in an effort to minimize variation. It also provided other comparative items, such as the average accuracy and time consumption. Particularly in the third group of studies, the time consumption performance was finished all at once, and other comparison elements such as total consumption time, feature extraction time, training time, and testing time were provided. Some requirements must be established in

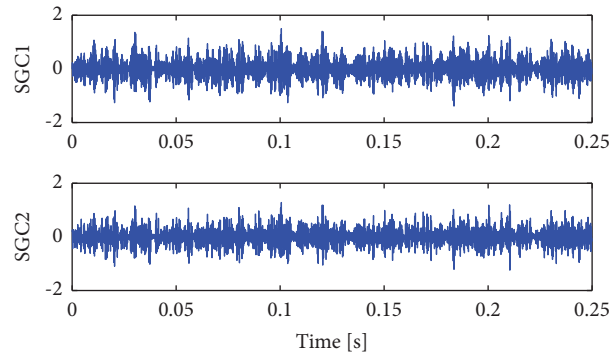

Figure 8: The decomposition components of the SGMD.

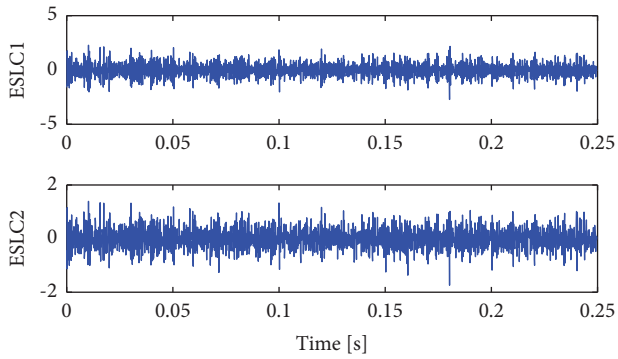

Figure 9: The decomposition components of the ESGMD-CC.

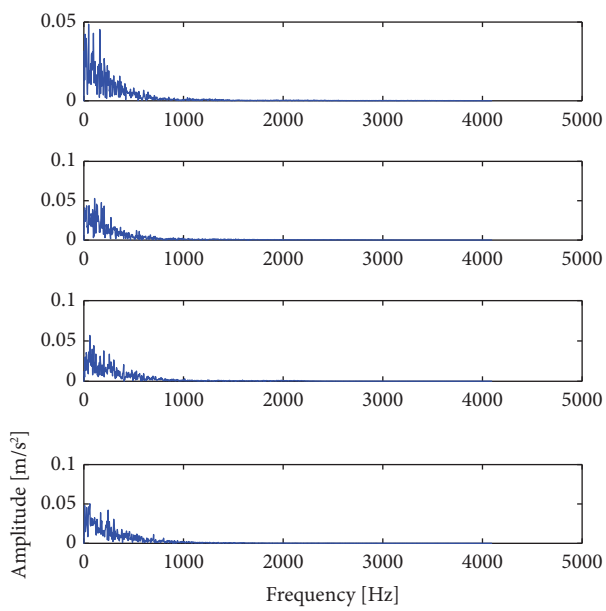

Figure 10: The envelope spectrums of the components of the VMD.

advance of the experiment. The threshold value ε_e set for calculating the cosine difference factor in equation (13) is 0.01%, the maximum pulse $f_{\max}$, the minimum pulse $f_{\min}$, the number of bats $M = 20$, the maximum loudness $A_{\max}$,

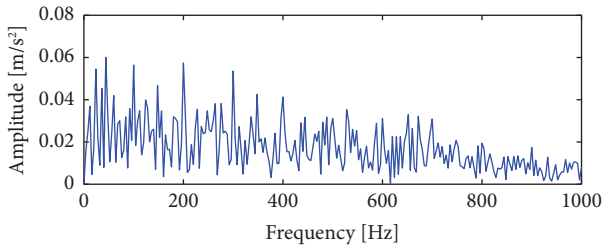

Figure 11: The envelope spectrums of the components of the SGMD.

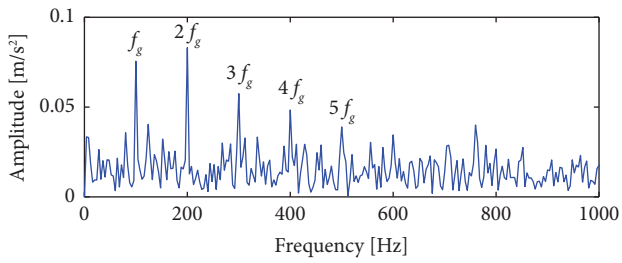

Figure 12: The envelope spectrums of the components of the ESGMD-CC.

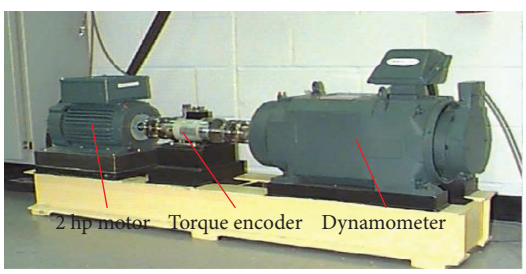

Figure 13: The experimental platform of the rolling bearing from the CWRU.

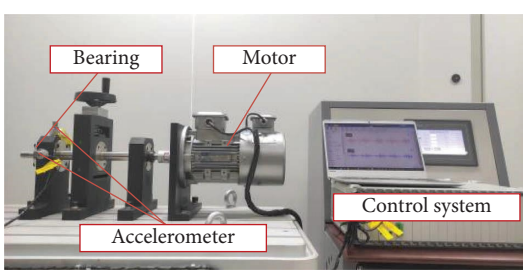

Figure 14: The experimental platform of the rolling bearing from the HFZZ-II.

the initial pulse emissivity $r_i^0 = 0.1$, and the maximum iteration number $P = 100$. In the experiment, the SVM experiment is completed by calling LIBSVM.

6.3. Results and Analysis. The initial set of comparative trials was conducted first. To assess if cosine difference factor and calculus operator limitations needed to be included, the enhanced ESGMD-CC was compared to the standard

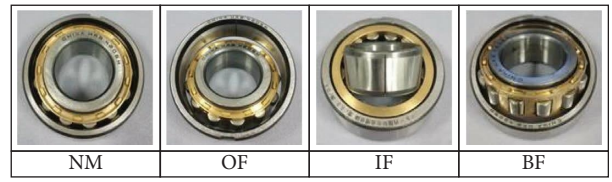

Figure 15: The four fault types of the rolling bearing.

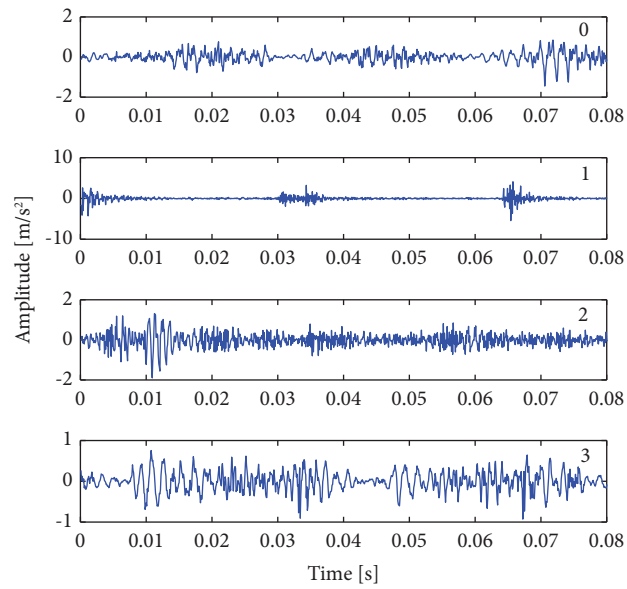

Figure 16: The time-domain waveform of the four fault types of the rolling bearing.

SGMD. In the event of an inner race fault, Figure 17 depicts the first four SGCs in a series of vibration signals, and Figure 18 depicts the final four SGCs. It is clear that the amplitude and energy proportion of the last four SGCs are lower in comparison. It may minimize the feature dimension, restrict the number of iterations, and effectively separate the noise components from the effective components by the restriction requirements of the cosine difference factor. They are contrasted with the enhanced ESGMD-CC because EEMD, LMD, and VMD are a few signal decomposition techniques frequently utilized in rotating machinery diagnostics. The feature extraction portion uses the power spectrum entropy-weighted singular values mapping approach, while the classification process outputs the diagnosis results by the BA-ELM model.

Visualization through the t-SNE mapping of the feature vectors acquired by various techniques is shown in Figure 19. It illustrates how distinct clustering effects are produced by various approaches, although it is not possible to determine the precise classification accuracy alone from this figure. The comparable experimental findings are displayed in Table 1. It demonstrates that the enhanced ESGMD-CC outperforms the competition in terms of diagnosis performance. This is mostly due to the fact that all ESLCs can enhance the fault features of the signal, hence reducing the feature dimension, while also retaining the

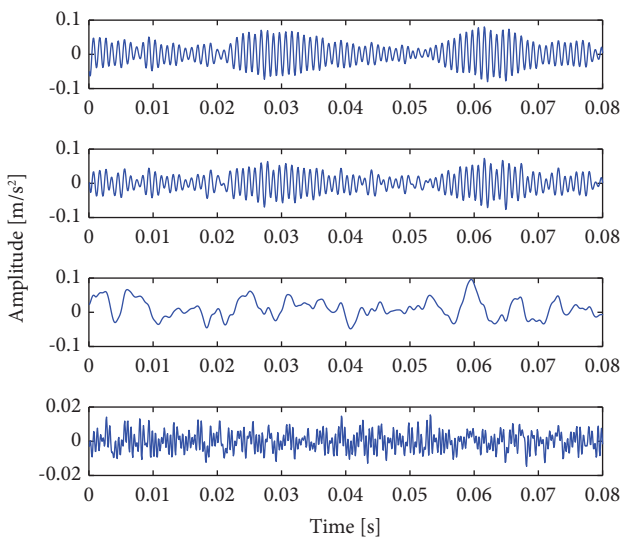

Figure 17: The first four SGCs of the SGMD.

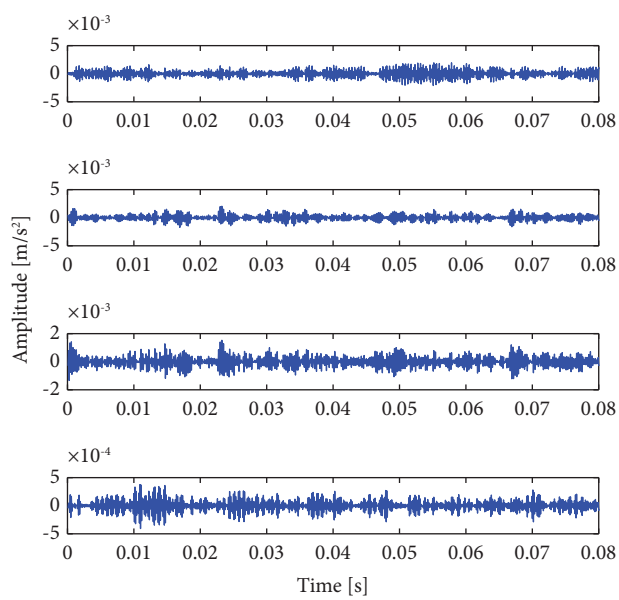

Figure 18: The last four SGCs of the SGMD.

helpful components and eliminating the useless ones in the process of limiting iteration and feature enhancement. The number of deconstructed modes is also shown at the same time. The enhanced ESGMD-CC has more decomposed components than other signal decomposition techniques, but far fewer than the traditional SGMD. The enhanced ESGMD-CC can successfully analyze and recreate the original signal's existing modes while preserving the phase space structure. More comprehensive and rich fault information is contained in its deconstructed components. The mapping method of power spectrum entropy-weighted singular values feature extraction is adopted, and the enhanced ESGMD-CC algorithm is fully combined to extract the feature values more effectively, which provides a necessary basis for the fault identification of the later classification algorithm. This is also the reason why the algorithm proposed in this paper has better diagnostic performance than other algorithms.

Next, a second set of comparative tests is conducted to assess how well classifiers and optimization methods work. The role of BA is to iteratively optimize the input weight and bias in the ELM model in the BA-ELM classifier in order to improve classification accuracy and generalizability. SVM and BP, two popular classification models, are also included in the comparison. Table 2 displays the results of the classification. In most experiments, it can be seen that the ELM model's classification accuracy is higher than that of other models following the feature extraction algorithm proposed in this paper and the classifier for fault recognition, and the model's diagnosis performance is more exceptional following BA optimization of the ELM parameters. In order to ensure that the two parameters of the ELM model are optimized, the input weight and hidden layer bias in the BA-ELM fault diagnosis model are modified based on the prediction error on the training set, and the output weight is further adjusted based on the above two parameters, allowing for faster and better convergence to the optimal solution, and thus has better classification accuracy and stronger generalization ability.

Of course, in addition to diagnostic accuracy, diagnostic efficiency and time consumed are also important factors in fault diagnosis. In order to evaluate the performance of the proposed method in terms of time consumption, the calculation time of the proposed method was compared in the third group of experiments. It mainly includes two levels: fault feature extraction (including signal decomposition and feature mapping) and fault classification (including training and optimization of the classifier, and fault discrimination of the classifier). Generally, the model only needs to be trained once and then put into use. This shows that the time for fault feature extraction and fault recognition of the classifier is more important than the time for training and optimization of the classifier. In this experiment, the training and optimization time of the classifier should also be compared, and we compare the fault feature extraction time, the fault recognition time of the classifier, and the overall consumption time. Table 3 displays the detailed results. It can be seen from the table that the test time of several methods is basically the same. Therefore, the total time is mainly spent on signal feature extraction and classifier training. The training time often depends on the optimization algorithm and the feature dimensions of the input classifier data, which are also added to Table 3 for comparison. For the SGMD and BA-ELM models without dimension reduction and improvement, the feature extraction time is relatively less and the training time is more due to the lack of relevant calculations such as dimension reduction. For the ESGMD-CC and BA-ELM models proposed in this paper, due to a series of operations such as cosine difference factor and feature enhancement, the feature extraction time is relatively large, and the training time is small due to the reduction of feature dimension. Generally speaking, the algorithm can only accomplish the best strategy by balancing the relationship between the two in order to have good performance in the

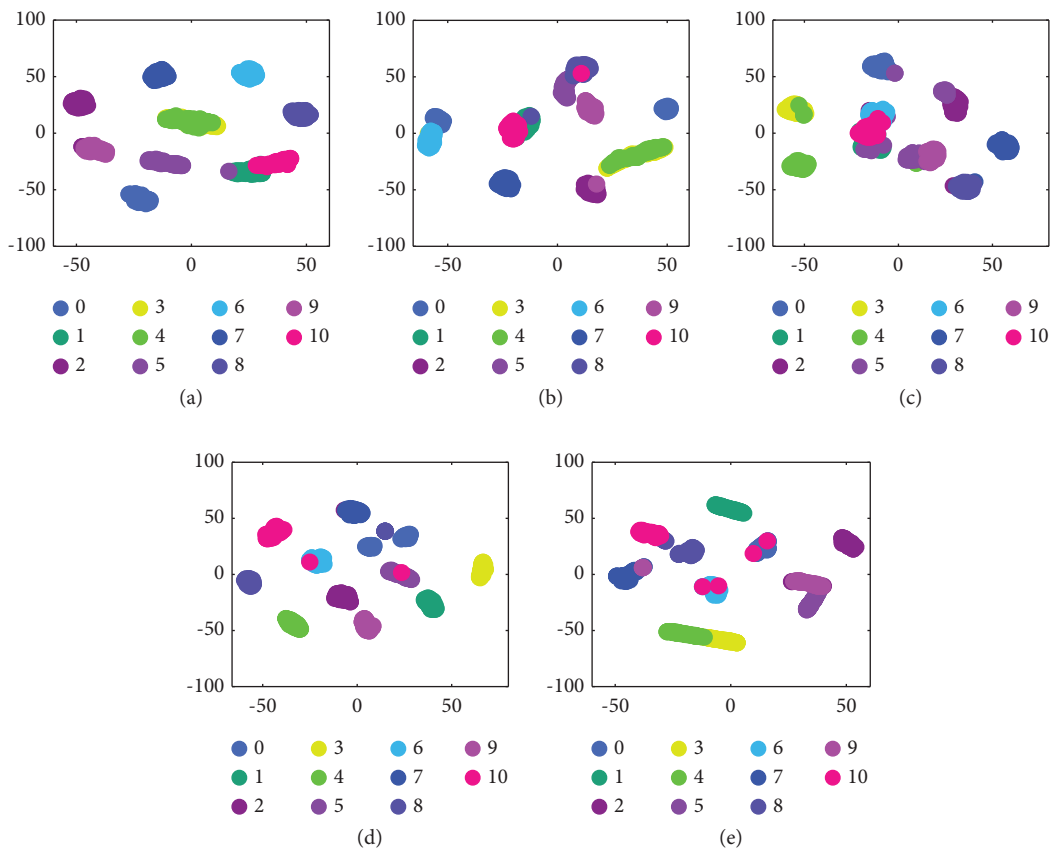

Figure 19: The t-SNE mapping after the feature extraction by different methods. (a) EEMD. (b) LMD. (c) VMD. (d) SGMD. (e) ESGMD-CC.

Table 1: The results of the first comparative experiments: evaluate the performance under different feature extraction methods.

Dataset	Methods	EEMD	LMD	VMD	SGMD	ESGMD-CC
CWRU	Feature dimension	11	5	7	341	23
	Accuracy (%)	92.95	86.81	96.13	97.05	98.41
HFZZ-II	Feature dimension	14	8	7	28	16
	Accuracy (%)	90.67	85.77	94.36	95.17	96.42

Table 2: The results of the second comparative experiments: evaluate the diagnostic.

Dataset	Methods	BP	SVM	ELM	BA-ELM
CWRU	Accuracy (%)	93.92	89.09	95.68	98.41
HFZZ-II	Accuracy (%)	91.48	88.35	92.95	96.42

time and accuracy required for the computation. The weights and bias for the unoptimized ELM model are produced at random through functions, which has some blindness and results in a generally subpar diagnosis performance. Its training duration decreases as a result of the lack of iterative optimization, but the diagnostic performance also suffers. The VMD algorithm is another typical signal extraction technique for feature extraction. VMD and BA-ELM algorithm is employed in this investigation. Although their feature dimensions are low, their feature extraction time and diagnosis time are higher than those of other methods. Among them, the experimental data in Table 3 were tested on the CWRU dataset containing 11 types of faults.

Many literatures also adopted the CWRU rolling bearing dataset for testing, and some literature also used other public dataset or self-built dataset for testing. In order to further prove the effectiveness of the proposed method, in the fourth group of experiments, some comparisons have been made to the published literature, as shown in Table 4. It can be seen that although the accuracy rates of the listed methods are different, they all have higher accuracy rates, and the test accuracy of the proposed method is higher than that of other methods. Compared with the feature extraction and classification algorithm without depth optimization in [37], the enhanced feature extraction algorithm and the iterative optimization classification model adopted in this paper should be outstanding in overall performance. The authors

Table 3: The results of the third comparative experiments: evaluate the time consumption between the current work and some other methods.

Methods	ESGMD-CC and BA-ELM	SGMD and BA-ELM	ESGMD-CC and ELM	ESGMD-CC and ELM	VMD and BA-ELM
Feature dimension	23	341	23	341	7
Accuracy (%)	98.41	97.05	95.68	94.51	96.13
Total (s)	304.77	240.77	299.68	233.51	348.91
Feature extraction (s)	299.61	233.45	299.61	233.45	343.79
Training (s)	5.15	7.31	0.06	0.05	5.11
Testing (s)	0.01	0.01	0.01	0.01	0.01

Table 4: The results of the fourth comparative experiments: comparative study between the proposed method of this article and the reported methods.

References	Methods	Dataset	Fault types	Accuracy (%)
(1). Ren et al. [34]	Sparse representation and SVM	CWRU	Ball fault (BF) Inner race fault (IF) Outer race fault (OF) Normal condition (NO)	94.11
(2). Li et al. [35]	DBN and 1D-CNN	Self-built	BF, IF, OF, and NO	97.50
(3). Gu et al. [36]	SDP-DCNN	Self-built	Outer ring crack Roller crack Inner ring crack Outer ring pitting Roller pitting Inner ring pitting	96.00
(4). Zhang et al. [37]	SGMD and SVM	CWRU	BF, IF, OF, and NO	96.23
(5). Authors of this paper	ESGMD-CC and BA-ELM	CWRU	BF, IF, OF, and NO	98.41

of [35] adopt a kind of depth network in which better diagnosis results can be obtained through the one-dimensional convolutional neural network. Through the method designed in this paper, its diagnostic performance is similar to that of the well-designed depth network model in terms of diagnostic accuracy.

The feature extraction and fault diagnosis model proposed in this paper, which combines ESGMD-CC and BA-ELM, have a better performance and are a viable rolling bearing fault detection approach, according to the aforementioned comparison studies.

7. Conclusions

This work presents an improved ESGMD-CC decomposition approach and a BA-ELM classification model for diagnosing rolling bearing faults. The vibration signal is first separated into many SGCs using SGMD in the proposed method, and then, the cosine difference factor and calculus operator constraint standards are used to reconstruct the SGCs. The power spectrum entropy-weighted singular values feature vectors are extracted from the obtained components as fault features to simplify the input to the subsequent classifier for fault identification. After the BA repeatedly improves the ELM parameters, the final classifier is generated for fault classification. The relevant comparison tests are performed on the bearing dataset to establish the method's diagnostic effectiveness. The experiment's findings are summarized as follows:

(1) The enhanced ESGMD-CC algorithm, which is based on Symplectic geometry similarity transformation, has better vibration signal decomposition performance and can effectively extract rich defect data from signals.

(2) The addition of the cosine difference factor efficiently lowers the feature dimension, separates the noise components, and reduces the number of SGMD decomposition iterations. The calculus operator is performed to improve the weak defect feature and make it simpler to extract.

(3) To extract the signal characteristics more efficiently, the enhanced ESGMD-CC is fully coupled with the mapping method of power spectrum entropy-weighted singular values feature extraction. It provides the necessary foundation for the later classification diagnosis.

(4) Iteratively optimizing the input weights and bias of the ELM model by the BA has better performance, and the diagnostic impact is superior to that of the unoptimized ELM, BP, and SVM models.

Data Availability

The data used to support the findings of this study are available from the corresponding author upon request.

Conflicts of Interest

The authors declare that they have no conflicts of interest.

Acknowledgments

This work was supported by the National Key Research and Development Project (Grant no. 2020YFE0204900), National Natural Science Foundation of China (Grant no. 62073193), Key Research and Development Plan of Shandong Province (Grant nos. 2021CXGC010204 and 2022CXGC020902), and the Fundamental Research Funds of Shandong University (Grant no. 2021JCG008).

References

[1] A. Faysal, W. K. Ngui, and M. H. Lim, "Noise eliminated ensemble empirical mode decomposition for bearing fault diagnosis," *Journal of Vibration Engineering and Technologies*, vol. 9, no. 8, pp. 2229–2245, 2021.

[2] D.-T. Hoang and H.-J. Kang, "A survey on Deep Learning based bearing fault diagnosis," *Neurocomputing*, vol. 335, pp. 327–335, 2019.

[3] S. Zhang, S. Zhang, B. Wang, and T. G. Habetler, "Deep learning algorithms for bearing fault diagnostics—a comprehensive review," *IEEE Access*, vol. 8, Article ID 29857, 2020.

[4] A. Had and K. Sabri, "A two-stage blind deconvolution strategy for bearing fault vibration signals," *Mechanical Systems and Signal Processing*, vol. 134, Article ID 106307, 2019.

[5] Z. Wang, G. Li, L. Yao, X. Qi, and J. Zhang, "Data-driven fault diagnosis for wind turbines using modified multiscale fluctuation dispersion entropy and cosine pairwise-constrained supervised manifold mapping," *Knowledge-Based Systems*, vol. 228, Article ID 107276, 2021.

[6] J. Wang, G. Du, Z. Zhu, C. Shen, and Q. He, "Fault diagnosis of rotating machines based on the EMD manifold," *Mechanical Systems and Signal Processing*, vol. 135, Article ID 106443, 2020.

[7] O. Karabiber Cura, S. Kocaaslan Atli, H. S. Türe, and A. Akan, "Epileptic seizure classifications using empirical mode decomposition and its derivative," *BioMedical Engineering Online*, vol. 19, no. 1, p. 10, 2020.

[8] R. Pathak, R. Kongari, and S. Joshi, "Low power design technique in passive tag to reduce the EMD noise for reliable communication with reader," in *Proceedings of the 2019 32nd International Conference on VLSI Design and 2019 18th International Conference on Embedded Systems (VLSID)*, pp. 454–458, Delhi, India, January 2019.

[9] H. Malik, Y. Pandya, and A. Parashar, "Feature extraction using EMD and classifier through artificial neural networks for gearbox fault diagnosis," *Applications of Artificial Intelligence Techniques in Engineering*, vol. 697, pp. 309–317, 2019.

[10] P. Zou, B. Hou, J. Lei, and Z. Zhang, "Bearing Fault diagnosis method based on EEMD and LSTM," *International Journal of Computers, Communications and Control*, vol. 15, no. 1, 2020.

[11] Y. Li, S. Si, Z. Liu, and X. Liang, "Review of local mean decomposition and its application in fault diagnosis of rotating machinery," *Journal of Systems Engineering and Electronics*, vol. 30, no. 4, pp. 799–814, 2019.

[12] Y. Xu, K. Zhang, C. Ma, S. Li, and H. Zhang, "Optimized LMD method and its applications in rolling bearing fault diagnosis," *Measurement Science and Technology*, vol. 30, no. 12, Article ID 125017, 2019.

[13] D. Goyal, A. Choudhary, J. K. Sandhu, P. Srivastava, and K. K. Saxena, "An intelligent self-adaptive bearing fault diagnosis approach based on improved local mean decomposition," *International Journal on Interactive Design and Manufacturing*, 2022.

[14] V. Sharma and A. Parey, "Extraction of weak fault transients using variational mode decomposition for fault diagnosis of gearbox under varying speed," *Engineering Failure Analysis*, vol. 107, Article ID 104204, 2020.

[15] J. Wang, Y. Zhang, F. Zhang et al., "Accuracy-improved bearing fault diagnosis method based on AVMD theory and AWPSO-ELM model," *Measurement*, vol. 181, no. 181, Article ID 109666, 2021.

[16] H. Li, T. Liu, X. Wu, and Q. Chen, "An optimized VMD method and its applications in bearing fault diagnosis," *Measurement*, vol. 166, Article ID 108185, 2020.

[17] H. Pan, Y. Yang, X. Li, J. Zheng, and J. Cheng, "Symplectic geometry mode decomposition and its application to rotating machinery compound fault diagnosis," *Mechanical Systems and Signal Processing*, vol. 114, pp. 189–211, 2019.

[18] H. Ren, W. Liu, M. Shan, and X. Wang, "A new wind turbine health condition monitoring method based on VMD-MPE and feature-based transfer learning," *Measurement*, vol. 148, Article ID 106906, 2019.

[19] X. Zhang, Y. Liang, J. Zhou, and Y. Zang, "A novel bearing fault diagnosis model integrated permutation entropy, ensemble empirical mode decomposition and optimized SVM," *Measurement*, vol. 69, pp. 164–179, 2015.

[20] F. Liu, J. Gao, and H. Liu, "The feature extraction and diagnosis of rolling bearing based on CEEMD and LDWPSO-PNN," *IEEE Access*, vol. 8, pp. 19810–19819, 2020.

[21] Z. Wang, L. Yao, Y. Cai, and J. Zhang, "Mahalanobis semi-supervised mapping and beetle antennae search based support vector machine for wind turbine rolling bearings fault diagnosis," *Renewable Energy*, vol. 155, pp. 1312–1327, 2020.

[22] M. Hosseinpour-Zarnaq, M. Omid, and E. Biabani-Aghdam, "Fault diagnosis of tractor auxiliary gearbox using vibration analysis and random forest classifier," *Information Processing in Agriculture*, vol. 9, no. 1, pp. 60–67, 2022.

[23] Z. Wang, G. Li, L. Yao et al., "Intelligent fault detection scheme for constant-speed wind turbines based on improved multiscale fuzzy entropy and adaptive chaotic Aquila optimization-based support vector machine," *ISA Transactions*, vol. 138, pp. 582–602, 2023.

[24] S. Pang, X. Yang, X. Zhang, and Y. Sun, "Fault diagnosis of rotating machinery components with deep ELM ensemble induced by real-valued output-based diversity metric," *Mechanical Systems and Signal Processing*, vol. 159, Article ID 107821, 2021.

[25] P. Liu and W. Zhang, "A fault diagnosis intelligent algorithm based on improved BP neural network," *International Journal of Pattern Recognition and Artificial Intelligence*, vol. 33, no. 9, Article ID 1959028, 2019.

[26] Y. Wei, Y. Yang, M. Xu, and W. Huang, "Intelligent fault diagnosis of planetary gearbox based on refined composite

hierarchical fuzzy entropy and random forest," *ISA Transactions*, vol. 109, pp. 340–351, 2021.

[27] F. Liu, J. Gao, and H. Liu, "A fault diagnosis solution of rolling bearing based on MEEMD and QPSO-LSSVM," *IEEE Access*, vol. 8, Article ID 101476, 2020.

[28] A. Dhini, I. Surjandari, B. Kusumoputro, and A. Kusiak, "Extreme learning machine – radial basis function (ELM-RBF) networks for diagnosing faults in a steam turbine," *Journal of Industrial and Production Engineering*, vol. 39, no. 7, pp. 572–580, 2021.

[29] G. Du, Q. Xu, and X. Yang, "Fault diagnosis of rotating machinery components using a deep kernel extreme learning machine under different working conditions," *Measurement Science and Technology*, vol. 31, no. 11, Article ID 115901, 2020.

[30] H. Du, D. Song, Z. Chen, H. Shu, and Z. Guo, "Prediction model oriented for landslide displacement with step-like curve by applying ensemble empirical mode decomposition and the PSO-ELM method," *Journal of Cleaner Production*, vol. 270, Article ID 122248, 2020.

[31] F. Liu, H. Wang, W. Li et al., "Fault diagnosis of rolling bearing combining improved AWSGMD-CP and ACO-ELM model," *Measurement*, vol. 209, Article ID 112531, 2023.

[32] J. He, F. Liu, X. Geng, X. Liang, F. Zhang, and M. Jiang, "Fault diagnosis method of rolling bearing based on ESGMD-CC and AFSA-ELM," *Structural Durability and Health Monitoring*, vol. 18, no. 1, pp. 37–54, 2024.

[33] Z. Yang, H. Zhang, S. Li, and C. Fan, "Prediction of residual gas content during coal roadway tunneling based on drilling cuttings indices and BA-ELM algorithm," *Advances in Civil Engineering*, vol. 2020, pp. 1–8, 2020.

[34] L. Ren, W. Lv, S. Jiang, and Y. Xiao, "Fault diagnosis using a joint model based on sparse representation and SVM," *IEEE Transactions on Instrumentation and Measurement*, vol. 65, no. 10, pp. 2313–2320, 2016.

[35] Y. Li, L. Zou, L. Jiang, and X. Zhou, "Fault diagnosis of rotating machinery based on combination of deep belief network and one-dimensional convolutional neural network," *IEEE Access*, vol. 7, pp. 165710–165723, 2019.

[36] Y. Gu, L. Zeng, and G. Qiu, "Bearing fault diagnosis with varying conditions using angular domain resampling technology, SDP and DCNN," *Measurement*, vol. 156, Article ID 107616, 2020.

[37] X. Zhang, C. Li, X. Wang, and H. Wu, "A novel fault diagnosis procedure based on improved symplectic geometry mode decomposition and optimized SVM," *Measurement*, vol. 173, Article ID 108644, 2021.